2017 IEEE International Conference on Robotics and Automation (ICRA)
Singapore, May 29 - June 3, 2017

Tunable Friction through Constrained Inflation of an Elastomeric Membrane

Kaitlyn P. Becker[1,2], Nicholas W. Bartlett[1,2], Melinda J. D. Malley[1,2], Peter M. Kjeer[1], Robert J. Wood[1,2]

Abstract— **Many areas of robotics, particularly locomotion and grasping, can benefit from the ability to modulate friction on surfaces that come into contact with objects in the environment. Previous research has tried to address the challenge of tunable friction; however, those efforts only provide modest gains or are difficult to integrate. We propose a tunable friction mechanism that relies on pneumatic actuation and is easily integrated into pre-existing soft actuators. We characterize the performance of our friction mechanism with quantitative force data for varying preload forces, substrate materials, and inflation pressures. Testing results show that our tunable friction mechanism achieves an order of magnitude differentiation in friction forces between high and low friction states. We demonstrate its potential application in a one degree-of-freedom soft crawler and a soft gripper with actuatable finger friction pads. The crawler successfully propelled itself forward by leveraging asymmetric strokes and the gripper achieved a factor of five differentiation of grip force between engaged and disengaged states of the friction tuning mechanism.**

I. Introduction

Friction is a central consideration in almost any robotic system, especially those involved in locomotion and/or grasping. A number of groups have used artificial microstructures similar to those of gecko setae to enhance friction in applications ranging from endoscopy to climbing robots [1], [2], [3], [4]. Others have examined fabrication techniques to make devices that enable directional friction [5]. While these techniques have demonstrated increased friction (and, in some cases, adhesion), the resulting systems are inherently passive. The addition of active friction control has the potential to further enhance the performance of these systems.

Tunable friction is especially intriguing for soft robotics. With regards to locomotion, being able to modulate the friction acting on a leg or foot could enable a single degree-of-freedom system to move forward by creating an asymmetric stroke [6]. For grasping, control over the friction of a gripper's fingers would allow for a simple actuation strategy: enable low friction to ease positioning of the gripper near the target, then increase friction when grasping. In both of these cases, adding a tunable friction mechanism could reduce the complexity of the control and actuation scheme.

The authors are aware of only a few studies regarding controllable friction in soft systems. Kim et al. have exploited shape memory polymers to achieve thermally controllable adhesion with actuation cycle times on the order of 100 seconds [7]. Lin et al. discuss a real-time mechanically tunable adhesive, though integration of this adhesive may be challenging in a fully soft system [8]. A self-assembling polymer network that creates a coating that modulates texture under UV light was described by Liu et al. [9]. Vikas et al., building on the work of Umedachi et al., have succeeded in creating soft crawling robots that leverage variable friction [10], [11]; their friction tuning mechanism is intimately coupled to the overall structure of the robot, enabling simple actuation though limiting the design space.

In contrast to this prior work, the mechanism proposed in this paper relies on local pneumatic actuation. This approach may have roots in biology, as geckos have been hypothesized to modulate pressure in their vasculature to aid in attachment to and release from substrates [12]. The mechanism proposed in this paper can be incorporated into a soft system in either a fully integrated or modular fashion. Directly integrating into the existing actuation and control systems of a pneumatic soft robot provides enhanced function with little to no additional complexity. Alternatively, when independent articulation is necessary, modularity enables separate control and actuation.

II. Design of the Mechanism

A. Principle of Operation

The proposed tunable friction mechanism consists of two main elements: an inflatable membrane and a restraining layer. The inflatable membrane is an elastomeric material that exhibits high friction, while the restraining layer is a relatively inextensible, low-friction material that features periodic holes. Before inflation, the restraining layer is in contact with a substrate of interest. When the membrane is inflated, it pushes through the holes in the restraining layer such that the elastomer contacts the substrate, thus enhancing friction. Schematics and photographs illustrating this mechanism can be seen in Fig. 1.

B. Model

A theoretical analysis using the Kirchhoff-Love theory for thin plates assisted in the choice of design parameters for the tunable friction mechanism. Because not all of the assumptions of this theory hold for large elastomeric deformation, the model was used to guide design rather than to precisely predict performance. The elastomer was modeled as a circular plate subject to a uniform pressure with a zero displacement boundary condition along the edge. With the assumption of an isotropic material, the governing equation simplifies to:

$$\nabla^2 \nabla^2 h = -\frac{P}{C} \tag{1}$$

[1]John A. Paulson School of Engineering and Applied Sciences, Harvard University, 60 Oxford Street, Cambridge, MA 02138

[2]Wyss Institute for Biologically Inspired Engineering, Harvard University, 3 Blackfan Circle, Boston, MA 02115

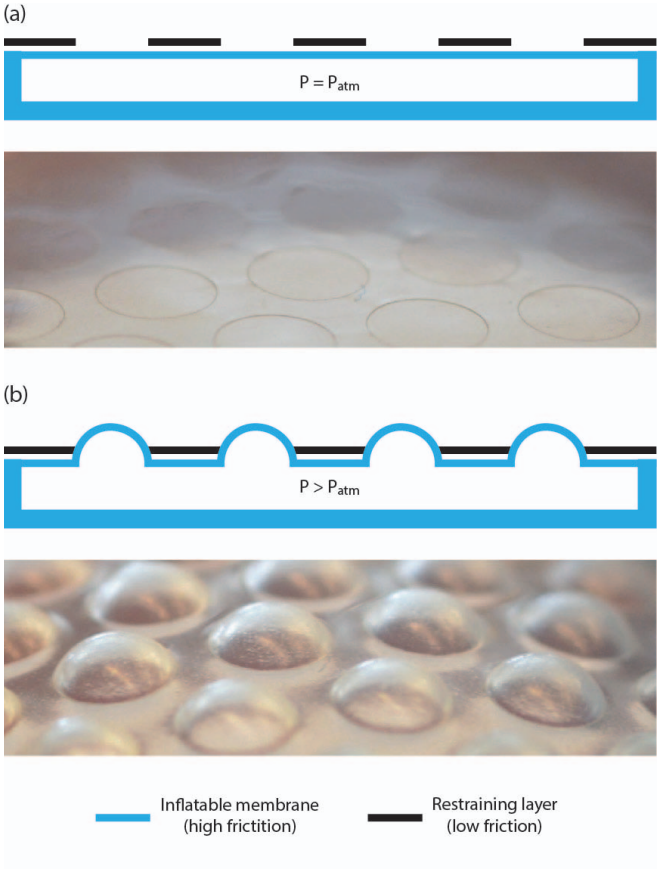

Fig. 1. (a) Before inflation, the membrane does not protrude beyond the thickness of the restraining layer, so the substrate only touches the low-friction restraining layer. (b) Upon inflation, the membrane pushes through the holes in the restraining layer, increasing the effective friction.

$$\text{where } C = \frac{2Et^3}{3\left(1-\nu^2\right)} \tag{2}$$

Here h is the maximum vertical deflection, P is the applied pressure, ν is the Poisson's ratio of the elastomer, E is the Young's modulus of the elastomer, and t is the elastomer thickness. Solving the above for h, we obtain:

$$h = \frac{3Pa^4\left(1-\nu^2\right)}{32Et^3} \tag{3}$$

where a is the radius of the hole in the restraining layer.

Equations (1) – (3) provide an analytic expression for the relationship between pressure, hole size, membrane thickness, and maximum deformation. This model does not account for deformation of the restraining layer that occurs at high inflation pressures, nor the deformation of the elastomer upon contact with an object. Nevertheless, the equations indicate feasible combinations of geometries and actuation pressures for the mechanism and prove useful in guiding design parameters.

C. Geometry and Materials

Preliminary testing with a number of different materials led us to use polydimethylsiloxane (PDMS) for the membrane material (Sylgard 184, Dow Corning). Regardless of the fabrication technique (in this work we used both molding and spin coating), all membranes were fabricated to be $200\,\mu\text{m}$ thick.

The restraining layer was fabricated from a $75\,\mu\text{m}$ thick polyester film (Dura-Lar, Grafix Arts). We chose this material for its inextensibility, low-friction, and ease of machinability. This particular thickness was chosen to ensure minimal plastic deformation upon actuation. We laser-cut the film with a hexagonal array of circular holes that were $3\,\text{mm}$ in diameter spaced $4\,\text{mm}$ apart (center-to-center). The size and spacing of the holes in the restraining layer were chosen in conjunction with the thickness and material of the inflatable membrane to enable actuation at a low pressure. As described by equation (3), a thinner (thicker) membrane could be used with smaller (larger) holes to achieve a similar actuation pressure. Two laser cutters were used for fabrication: a diode-pumped solid state (DPSS) laser (E-355, Oxford Lasers Ltd.), and a CO_2 laser (VLS 6.60, Versa Laser).

From equation (3) in the preceding section, the calculated actuation pressure required for the membrane to extend up to the thickness of the restraining layer is approximately $0.7\,\text{kPa}$. To extend one millimeter beyond the restraining layer, an actuation pressure of approximately $9.7\,\text{kPa}$ is required. For a point of comparison, a typical soft bending actuator performs at $69\,\text{kPa}$ [13].

III. Mechanism Testing

A. Testing Setup

We characterized the tunable friction mechanism performance on a universal testing machine (Instron 5544, Instron) to measure friction forces with varying preload forces, substrate materials, and inflation pressures. To facilitate characterization and mounting to the Instron, we made a soft friction tuning device coupled to a rigid fixture. The friction tuning device consisted of an inflatable elastomer bladder with one ($200\,\mu\text{m}$ thick) side that was in contact with a polyester restraining layer. The bladder was cast as a single piece of PDMS using a mold made from a stack of laser-cut acrylic plates and $200\,\mu\text{m}$ stainless steel shim stock to precisely control the membrane thickness. The restraining layer and bladder were mounted in a rigid acrylic fixture and clamped together with fasteners. A pneumatic line was plumbed into an inflation port in the side of the elastomer bladder to provide pressure. A schematic and photograph of the friction device can be seen in Fig. 2.

The friction tuning device was incorporated into a custom Instron fixture designed to enable measurement of horizontal friction forces. This lateral pulling configuration was used in place of the typical vertical setup to minimize off-axis loads applied to the load cell of the Instron and to simplify testing procedures. A pneumatic cylinder mounted to the Instron fixture allowed measurements to be made under a variety of preload forces. Because the friction tuning device remained stationary, the substrate of interest was fixed to a mobile sled. The top of the mobile sled was in contact with the inflatable membrane, and its bottom was coated with Teflon. To minimize the influence of frictional forces from sources other than the inflatable membrane on the substrate

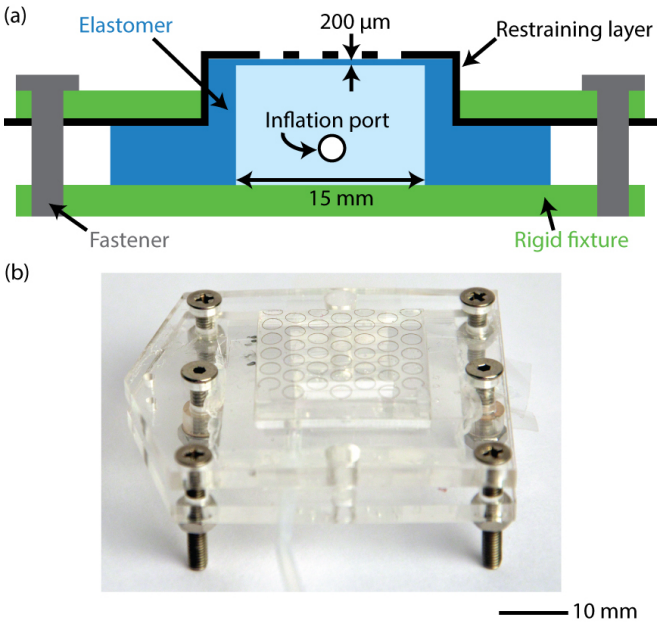

Fig. 2. A (a) schematic and (b) photograph of the friction tuning device used for mechanical testing on the Instron. Note that the device is oriented upside-down (to highlight the friction tuning features); in actual testing the restraining layer would be on the bottom as to be in contact with the substrate of interest.

of interest, the mounting plate for the Instron fixture was also coated in Teflon, providing a Teflon-Teflon interface between the mobile sled and the Instron fixture mounting plate. The mobile sled was attached to a $0.64\,\mathrm{mm}$ diameter Kevlar string that, through a pulley, connected to the moving stage of the Instron. As the Instron stage moved, the load cell measured the force required to counteract the friction applied by our friction tuning device. The Instron fixture used for the testing is illustrated in Fig. 3.

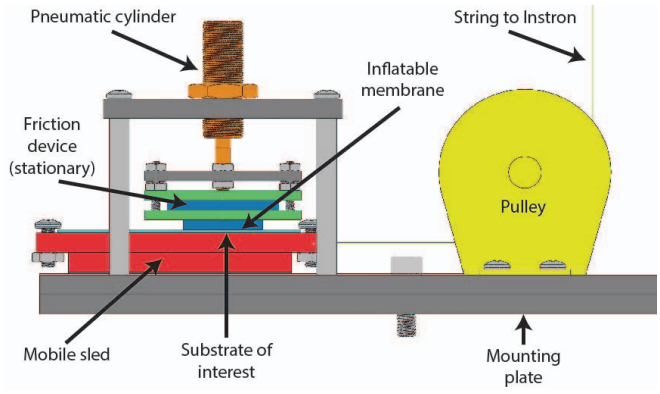

Fig. 3. A schematic of the Instron fixture setup used to measure horizontal friction forces. The friction tuning device (with the inflatable membrane) remains stationary and is pressed downwards into the mobile sled via a pneumatic cylinder. The mobile sled, which carries the substrate of interest, is pulled by the Instron through a pulley.

B. Tests Performed

The effects of three variables (preload force, substrate material, and inflation pressure) on the performance of our friction tuning device were measured on the Instron. Preload forces were applied to the friction device via the pneumatic cylinder, which was controlled with a regulated pressure supply. We calculated the preload force as the pressure applied to pneumatic cylinder multiplied by the cylinder bore.

1) Effect of preload force: In the first series of tests, we applied a constant preload force to the friction device and performed a ramping lateral pull force test ($10\,\mathrm{N/min}$) with the Instron. Each of these tests was performed on a glass substrate. We then determined the pull force at which the device began to slip. This test was conducted at three preload forces (2.46, 4.91, and $7.37\,\mathrm{N}$), as well as four inflation pressures (0, 13.79, 27.58, and $41.37\,\mathrm{kPa}$).

2) Effect of substrate material: In a second series of tests, again using a ramping force profile, we maintained a single preload force ($4.91\,\mathrm{N}$) but varied the substrate material and inflation pressure. This second set of tests compared the effect of glass, Teflon, and stainless steel substrates.

3) Effect of inflation pressure: We conducted a final set of tests to explore the friction differential between the unactuated and actuated states of the friction tuning device. With the Instron programmed to move with a constant rate of extension ($10\,\mathrm{mm/min}$), we allowed the device to slide on a glass substrate in its unactuated state. After a short delay, we exerted a step input to the inflation pressure up to various values (13.79, 27.58, and $41.37\,\mathrm{kPa}$). We recorded the average value for the force measured by the load cell before and after the step input (corresponding, respectively, to the unactuated and actuated states as recorded in Table I). This test was also repeated at different preload forces (2.46, 4.91, and $7.37\,\mathrm{N}$).

C. Results

1) Effect of preload force: The friction forces shown in Fig. 4 suggest that the effect of preload force is minimal compared to other effects (see below). The preload force does, however, influence the efficacy of increasing the inflation pressure.

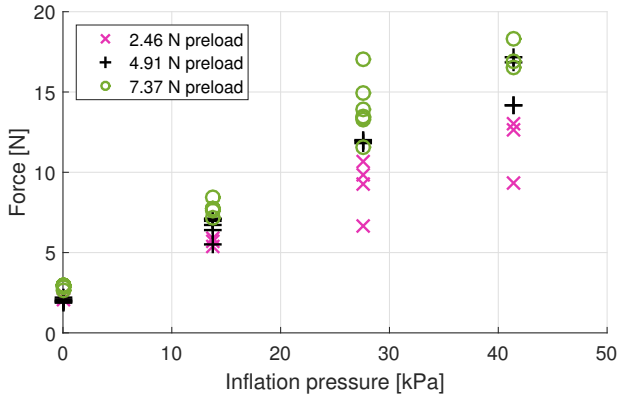

Fig. 4. Graph of friction force data as a function of inflation pressure for different preloads, as measured on the Instron. These tests were performed on a glass substrate. Note that, for all conditions, each inflation pressure was tested at least three times.

2) Effect of substrate material: The effect of varying substrate material for a given preload force and varying inflation pressures is shown in Fig. 5. As expected, the friction tuning device exerts lower frictional forces when applied to slippery surfaces such as Teflon. Higher-order effects that do not scale with inflation pressure, such as tribological variables or adhesion forces (e.g. van der Waals, bulk electrostatic, or capillary), may also be present; these effects could be an interesting area of future study. However, for all substrates, we do see that there is a significant increase in friction with any nonzero inflation pressure.

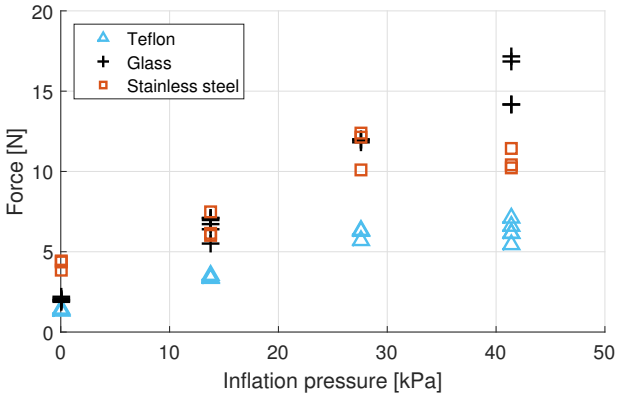

Fig. 5. Graph of friction force data as a function of inflation pressure for different substrates, as measured on the Instron. These tests were performed with a constant preload force of 4.91 N. Note that, for all conditions, each inflation pressure was tested at least three times.

TABLE I
RESULTS OF FRICTION DIFFERENTIAL TESTING

Preload Force [N]	Inflation Pressure [kPa]	Unactuated Force [N]	Unactuated CoF* [–]	Actuated Force [N]	Actuated CoF* [–]
2.46	27.58	1.14	0.46	12.15	4.94
2.46	27.58	1.27	0.52	12.50	5.08
2.46	27.58	1.43	0.58	12.82	5.21
4.91	13.79	2.16	0.44	7.26	1.48
4.91	13.79	2.01	0.41	7.78	1.58
4.91	13.79	2.77	0.56	8.57	1.74
4.91	27.58	2.66	0.54	13.46	2.74
4.91	27.58	2.82	0.58	14.49	2.95
4.91	27.58	2.25	0.46	14.69	2.99
4.91	41.37	1.77	0.36	18.88	3.85
4.91	41.37	1.73	0.35	20.04	4.08
4.91	41.37	1.80	0.37	19.35	3.94
7.37	27.58	2.68	0.36	15.94	2.16
7.37	27.58	3.31	0.45	16.54	2.24
7.37	27.58	3.38	0.46	17.05	2.31

This table details the change in the frictional force (for a given preload force and inflation pressure) that occurs as the friction device is actuated on a glass substrate. The data are available to compare across inflation pressures for a given preload force as well as across preload forces for a given inflation pressure. One can see a much stronger dependence on inflation pressure than preload force. *CoF denotes the coefficient of friction.

3) Effect of inflation pressure: As alluded to above, the inflation pressure has a much more substantial effect than preload force on the measured friction forces. The increase in friction force measured between our unactuated and actuated friction device on glass exceeds an order of magnitude in some conditions, as shown in Table I. Note that the data reported allow one to see the effects from variation in preload force with constant inflation pressure as well as the effects from variation in inflation pressure with constant preload force. The stronger dependence on inflation pressure is attractive for applications like crawling or grasping, where it may be advantageous for friction forces to be relatively insensitive to crawler weight or grasping force, and more sensitive to a controllable variable such as internal pressure.

In addition to considering frictional force, we can examine the effect of preload force and inflation pressure on the coefficient of friction (see Table I). The coefficients of friction are simply the frictional forces divided by the preload forces. From this perspective, the data show that higher coefficients of friction are achieved at lower preload forces, which is beneficial for soft robotics given the typically low forces involved.

IV. Implementation in a Crawling Robot

To test its effectiveness, we incorporated our tunable friction mechanism into a crawling robot, which can be seen in Fig. 6. The robot consists of a body and two legs. Each leg is a pneumatic bending actuator, similar to the ones used in other soft robotic applications [13], that has been modified to accommodate tunable friction pads. The friction pads rely on the same mechanism as above, consisting of a polyester restraining layer and an inflatable PDMS membrane. A second polyester sheet serves as a backing to the membrane, completing the inflatable structure. We sealed the membrane to the polyester backing with a silicone adhesive (Loctite Superflex Clear RTV, Henkel Corp.), and then sewed the edges with cotton thread for reinforcement. If stronger adhesion between these layers is required, success has been found by using silane treatment and oxygen plasma to bond PDMS to plastics [14], [15]. The friction pads were mechanically attached to the sides of the legs with an air port protruding into the internal cavity of the leg, thereby creating a direct pneumatic coupling and resulting in a single degree-of-freedom system.

Upon inflation, the friction pads actuate first (at approximately 7 kPa), providing a pivot point for each leg. Upon increasing the pressure, the legs begin to bend (at approximately 35 kPa), pushing the robot forward. When quickly vented, the friction pads and legs deflate simultaneously, allowing the elastomeric membrane of the friction pads to retract as the legs return to their initial, unactuated state. Without the high friction pivot points at the distal ends, the legs sweep back to their unactuated state without pushing the robot body backwards.

This crawling robot was tested on a glass substrate (see Fig. 6 and Supplemental Video). With an actuation frequency of $0.5\,\mathrm{Hz}$, the crawler was able to propel itself forward at a speed of 0.2 body lengths per second ($12\,\mathrm{mm/s}$). To confirm the utility of our friction pads, we tried operating the crawling robot with small polyester sheets under the friction pads, effectively neutralizing our tuning mechanism. Additionally, we attempted crawling with legs made from unaltered bending actuators (i.e. without any friction pads). We found that after numerous actuation cycles, neither modified robot was able to produce any net motion, proving the necessity of our tunable friction mechanism for locomotion in this configuration.

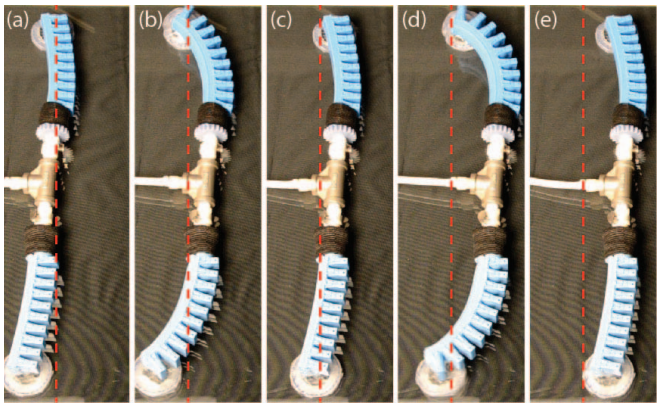

Fig. 6. (a) The crawler in its initial state. Each leg consists of a bending actuator with a tunable friction pad at its distal end. (b) As the legs actuate during the power stroke, the friction pads engage, creating pivot points that allow the body of the robot to move forward. (c) As the legs are vented, the friction pads depressurize and the high-friction membrane retracts. With the low-friction restraining layer now in contact with the substrate, the friction pads slide forward with the legs in the return stroke, resulting in net forward motion. Frames (d) and (e) show another cycle. The dashed line serves as a position reference.

V. Integration with a Soft Gripper

As a second demonstration, we created a soft robotic gripper that has the ability to modulate the friction of its fingers, which can be seen in Fig. 7. Each finger of the gripper is a pneumatic bending actuator with a tunable friction pad attached to its fingertip. The friction pads are made of two layers of PDMS bonded together with oxygen plasma treatment. For a restraining layer, we used thermoplastic polyurethane (TPU) coated taffeta (heat sealable taffeta, Seattle Fabrics). We deviated from our typical restraining layer choice of polyester in this demonstration to take advantage of certain properties of the taffeta that aid in integration with the soft bending actuator; the ability to tailor the restraining layer material to the specific needs of the application speaks to the versatility of our fabrication process. In addition to serving as the restraining layer for the inflatable membrane, the taffeta also mechanically secures the friction pads to the bending actuators and helps reinforce the body of the actuator.

In contrast to the crawling robot discussed in the preceding section, the friction pads in this demonstration are actuated independently from the main bending actuators. That is, this gripper is a multiple degree-of-freedom system with independent control over finger actuation and friction modulation. The friction pads actuate at approximately $7\,\mathrm{kPa}$, whereas the fingers are fully actuated at approximately $55\,\mathrm{kPa}$. If found to be advantageous, the system could be redesigned with only minimal effort to directly couple the actuation of the fingers and the friction pads. As seen previously, the actuation pressure of the friction pads has a strong dependence on both membrane thickness and restraining layer hole size, so altering these parameters is a simple way to modulate actuation pressure of the friction pads.

Using the gripper setup shown in Fig. 7, we successfully positioned a light bulb into a mating socket (see Supplemental Video). By switching between actuated and unactuated friction states, the gripper slid over the surface of the bulb to adjust its gripping position while still cradling and preventing the light bulb from falling.

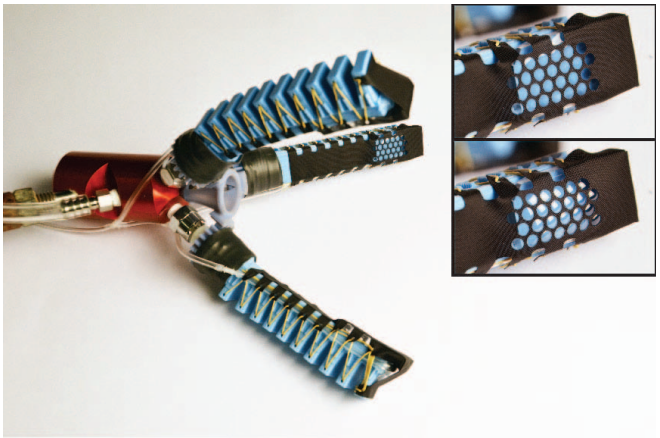

Fig. 7. The gripper consists of pneumatic bending actuators that have been modified with friction pads at the fingertips. The friction pads are made of two layers of PDMS plasma bonded together. The taffeta anchors the friction pad to the bending actuator and serves as a restraining layer for the inflatable membrane. The two inset pictures show the friction pads unactuated (top) and actuated (bottom).

To evaluate the tunable friction performance of the soft gripper, we measured the force required to remove a plastic cylinder from its grasp with both actuated and unactuated friction pads. With the Instron programmed to move at a constant rate ($50\,\mathrm{mm/min}$), the grasp forces were measured for three cylinder diameters (25.4, 50.8, and $76.2\,\mathrm{mm}$). The bending actuators were pressurized to $75.8\,\mathrm{kPa}$ and the friction pads were pressurized to $17.2\,\mathrm{kPa}$ for each of the tests. A picture of the test setup is shown in Fig. 8 and the force data is shown in Fig. 9. The plot shows the average values from the testing, as well as one standard deviation above and below the average values. As expected, the peak forces recorded as the cylinder slips through the actuated friction pads (represented by the solid lines) are much higher than those from the cylinder slipping through the same pair of pneumatic bending actuators with unactuated friction pads (represented as dashed lines).

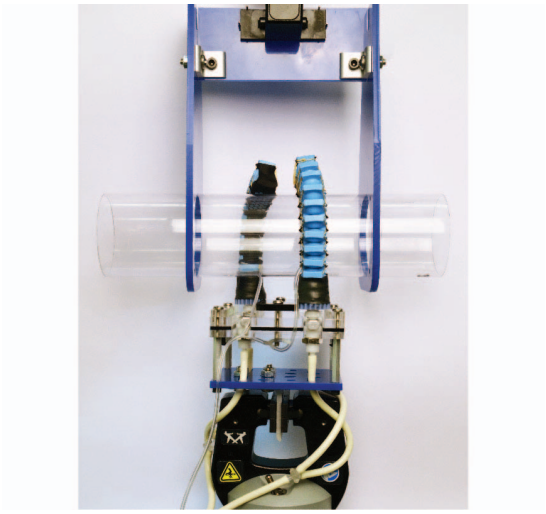

Fig. 8. Instron test setup used to measure the force require to pull cylinders of various diameters. The two bending actuators feature friction pads on their fingertips, which were tested in both actuated and unactuated states.

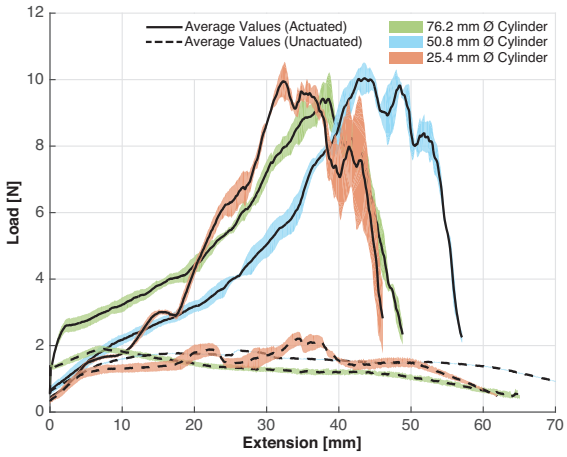

Fig. 9. Forces required to pull cylinders of varying sizes from between two bending actuators with actuated (solid lines) and unactuated (dashed lines) friction pads. The shaded regions show one standard deviation above and below the average values (n = 5). In all tests, the bending actuators and friction pads were pressurized to 75.8 kPa and 17.2 kPa, respectively.

VI. Conclusions

In this work we have demonstrated the benefits of tunable friction for robotic systems. Our fabrication strategy has proven to be simple, robust, and applicable in several scenarios. We have shown through quantitative force testing that our tunable friction mechanism increases friction beyond an order of magnitude between unactuated and actuated states.

We have highlighted the performance of this mechanism in two demonstrations. In the first, we fabricated a simple crawling robot that consisted of two pneumatic bending actuators outfitted with tunable friction pads. Relying on the fact that the friction pads actuated at a lower pressure than the bending actuators, this single degree-of-freedom robot propelled itself forward through asymmetric friction on the power and return strokes. In the second demonstration, a multiple degree-of-freedom soft gripper was shown to modulate its grasp force by a factor of five between the unactuated and actuated states of the friction pads. Using only this friction differential, the gripper was able to successfully screw in a light bulb.

Acknowledgment

This work was supported by the Wyss Institute for Biologically Inspired Engineering; the National Science Foundation (under award 1556164); the Army Research Office, National Defense Science and Engineering Graduate (NDSEG) Fellowship; and the National Science Foundation Graduate Research Fellowship (under grant DGE1144152). In addition, the prototypes were enabled by equipment supported by the ARO DURIP program (under award W911NF-13-1-0311). Any opinions, findings, conclusions, or recommendations expressed in this material are those of the authors and do not necessarily reflect those of the funding organizations.

References

[1] E. Buselli, V. Pensabene, P. Castrataro, P. Valdastri, A. Menciassi, and P. Dario, "Evaluation of friction enhancement through soft polymer micro-patterns in active capsule endoscopy," *Measurement Science and Technology*, vol. 21, no. 10, p. 105802, 2010.

[2] P. Glass, E. Cheung, and M. Sitti, "A legged anchoring mechanism for capsule endoscopes using micropatterned adhesives," *IEEE Transactions on Biomedical Eng.*, vol. 55, no. 12, pp. 2759–2767, 2008.

[3] D. Santos, B. Heyneman, S. Kim, N. Esparza, and M. R. Cutkosky, "Gecko-inspired climbing behaviors on vertical and overhanging surfaces," in *Robotics and Automation, 2008. ICRA 2008. IEEE International Conference on*, pp. 1125–1131, IEEE, 2008.

[4] B. Aksak, M. P. Murphy, and M. Sitti, "Gecko inspired micro-fibrillar adhesives for wall climbing robots on micro/nanoscale rough surfaces," in *Robotics and Automation, 2008. ICRA 2008. IEEE International Conference on*, pp. 3058–3063, IEEE, 2008.

[5] P. Day, E. V. Eason, N. Esparza, D. Christensen, and M. Cutkosky, "Microwedge machining for the manufacture of directional dry adhesives," *Journal of Micro and Nano-Manufacturing*, vol. 1, no. 1, p. 011001, 2013.

[6] C. Majidi, R. F. Shepherd, R. K. Kramer, G. M. Whitesides, and R. J. Wood, "Influence of surface traction on soft robot undulation," *Int. Journal of Robotics Research*, vol. 32, no. 13, pp. 1577–1584, 2013.

[7] S. Kim, M. Sitti, T. Xie, and X. Xiao, "Reversible dry micro-fibrillar adhesives with thermally controllable adhesion," *Soft Matter*, vol. 5, no. 19, pp. 3689–3693, 2009.

[8] P.-C. Lin, S. Vajpayee, A. Jagota, C.-Y. Hui, and S. Yang, "Mechanically tunable dry adhesive from wrinkled elastomers," *Soft Matter*, vol. 4, no. 9, pp. 1830–1835, 2008.

[9] D. Liu and D. J. Broer, "Self-assembled dynamic 3d fingerprints in liquid-crystal coatings towards controllable friction and adhesion," *Angewandte Chemie Int. Ed.*, vol. 53, no. 18, pp. 4542–4546, 2014.

[10] V. Vikas, E. Cohen, R. Grassi, C. Sozer, and B. Trimmer, "Design and locomotion control of soft robot using friction manipulation and motor-tendon actuation," *arXiv preprint arXiv:1509.06693*, 2015.

[11] T. Umedachi, V. Vikas, and B. A. Trimmer, "Highly deformable 3-d printed soft robot generating inching and crawling locomotions with variable friction legs," in *2013 IEEE/RSJ International Conference on Intelligent Robots and Systems*, pp. 4590–4595, IEEE, 2013.

[12] A. P. Russell, "Descriptive and functional anatomy of the digital vascular system of the tokay, gekko gecko," *Journal of Morphology*, vol. 169, no. 3, pp. 293–323, 1981.

[13] K. C. Galloway, K. P. Becker, B. Phillips, J. Kirby, S. Licht, D. Tchernov, R. J. Wood, and D. F. Gruber, "Soft robotic grippers for biological sampling on deep reefs," *Soft Robotics*, vol. 3, no. 1, pp. 23–33, 2016.

[14] L. Tang and N. Y. Lee, "A facile route for irreversible bonding of plastic-pdms hybrid microdevices at room temperature," *Lab on a Chip*, vol. 10, no. 10, pp. 1274–1280, 2010.

[15] V. Sunkara, D.-K. Park, and Y.-K. Cho, "Versatile method for bonding hard and soft materials," *RSC Advances*, vol. 2, no. 24, pp. 9066–9070, 2012.